The International Journal of Advanced Manufacturing Technology (2018) 95:4129–4140
https://doi.org/10.1007/s00170-017-1493-5

ORIGINAL ARTICLE

Experimental study of chemical mechanical polishing of the final surfaces of cemented carbide inserts for effective cutting austenitic stainless steel

Zihua Hu[1] · Changjiang Qin[1] · Zezhong C. Chen[2] · Zhiping Yang[1,3] · Tao Fang[1] · Meijiao Mao[1]

Received: 27 March 2017 / Accepted: 17 December 2017 / Published online: 5 January 2018

Abstract
Defects of the final surfaces of cemented carbide inserts by means of conventional grinding method include grinding burn, crack, and thermal deformation, causing low cutting efficiency. To address the problems of the conventional way in grinding the insert surfaces, the chemical mechanical polishing (CMP) process is adopted in finish machining rake faces. First, the CMP process parameters are optimized with orthogonal experiments and Taguchi's method, and the cemented carbide insert surfaces are made with 14.399 nm Ra of its rake face. Second, the inserts made with the conventional grinding and the CMP methods are used to lathe 1Cr18Ni9Ti austenitic stainless steel. Under the same cutting conditions, the cutting forces of the polished insert is less than those of the grinding insert, the cutting time of the polished insert is longer than that of the grinding insert, and the average life of the polished insert is 32.3% longer than that of the grinding insert. Finally, the scanning electron microscopy (SEM) and the energy dispersive spectroscopy (EDS) analysis have shown that the polished insert rake face has less adhesive wear , abrasive wear, and minor oxidation wear compared to the wear of the grinding insert rake face. This study demonstrates that the CMP is a potential way of processing the insert surfaces in the tooling industry.

Keywords Cemented carbide inserts · Chemical mechanical polishing (CMP) · Austenitic stainless steel · Cutting performance

1 Introduction

With high wear resistance, hardness, and strength, cemented carbide inserts are widely used in the automobile, aerospace, and construction machinery manufacturing. To achieve high and ultra-high speed machining, precision mold and tool manufacturing, nano and micro machining, and carbide insert quality should be even better. The insert material and geometric parameters and the insert surface quality are important to the insert quality [1]. The insert surface is finally machined with diamond grinding in various conditions, such as dry [2], wet [3], electrochemical [4], and electrolytic in-process dressing (ELID) grinding [5]. However, the thermal deformation, grinding burn, and surface or subsurface damage (such as deformation layer, surface or subsurface crack, and residual stress) occur on the insert surface [6], and these defects seriously affect the tool performance and life. It is necessary to develop a new method of finish machining insert surfaces to reduce the insert surface deformation, the grinding burn, and surface or subsurface damage. Chemical mechanical polishing (CMP) is a new technology known to provide global planarization of topography with a low post-planarization slope [7]. This method has advantages of good machined surface quality, no surface or subsurface damage, low density of surface defect, and low cost [8], and has been widely used to precision and ultra-precision machining for Al [9], Cu [10], W [11], and other metals and their alloy materials [12].

✉ Zihua Hu
iamtxtu@163.com

[1] School of Mechanical Engineering, Xiangtan University, Xiangtan, Hunan, People's Republic of China

[2] Department of Mechanical and Industrial Engineering, Concordia University, Montreal, Quebec, Canada

[3] Zhuzhou Cemented Carbide Cutting Tools Co. Ltd., Zhuzhou, Hunan, People's Republic of China

Fig. 1 The chosen insert type

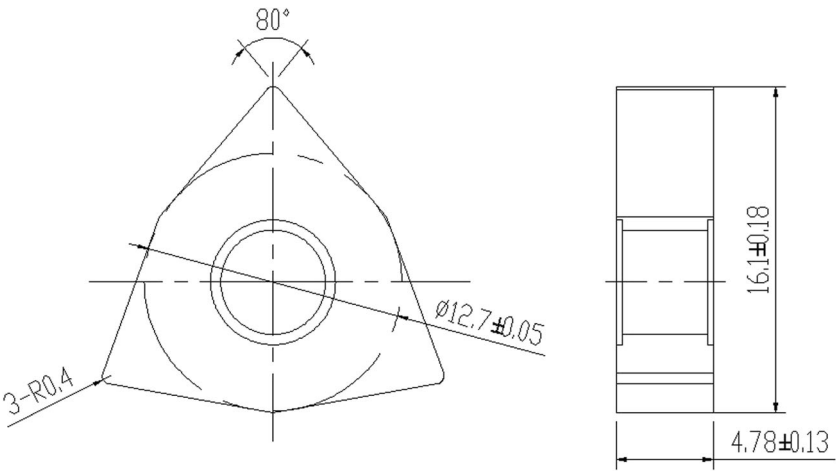

Table 1 Chemical composition and mechanical properties of the YG8 insert

Material	Component	Hardness (HRA)	Flexural strength (MPa)	Elastic modulus (GPa)	Density (g/cm^3)
YG8	w_{WC} 92%, w_{Co} 8%	89.0	1670	600	14.7

Fig. 2 Nanopoli-100 polisher

In this work, first, the process parameters of chemical mechanical polishing of the insert rake face are optimized with orthogonal experiments and Taguchi's method. The optimal CMP process is applied to the inserts. Second, the inserts made with the conventional grinding and the CMP methods are used to lathe 1Cr18Ni9Ti austenitic stainless steel. Finally, the scanning electron microscopy (SEM) and the energy dispersive spectroscopy (EDS) analysis are conducted.

2 Experimental method

2.1 CMP test of cemented carbides inserts

The YG8 cemented carbide insert is chosen as the CMP test object, which has been processed by means of rough grinding. The drawing of the chosen insert type is shown in Fig. 1. Its chemical composition and mechanical properties are given in Table 1.

The nanometer Nanopoli-100 polisher is used to polish the YG8 inserts, which is shown in Fig. 2. In the CMP experiment of the inserts, the rough polishing, semi-polishing, and fine polishing orthogonal experiments are used to preprocess the rake face of the inserts, and the volume fraction of H_2O_2 in the polish slurry is 10%, the particle concentration of rough and semi-polishing is 25%wt. The experimental factors and factor

Table 2 Experimental factors and factor levels of rough polishing

Levels	A, S_iC abrasive particle (um)	B, Polishing speed (rpm)	C, Polishing pressure (kPa)	D, Polishing time (min)
1	26	40	158	35
2	22	50	177.8	50
3	18	60	197.5	65

Table 3 Experimental factors and factor levels of semi-polishing

Levels	A, S_iC abrasive particle (um)	B, Polishing speed (rpm)	C, Polishing pressure (kPa)	D, Polishing time (min)
1	10	30	98.75	25
2	7	35	118.5	35
3	5	40	138.25	45

Table 4 Experimental factors and factor levels of fine polishing

Levels	A, Diamond powder (um)	B, Polishing speed (rpm)	C, Polishing pressure (kPa)	D, Polishing time (min)	E, Abrasive concentration (ct/ml)
1	0.5	20	39.5	20	0.181
2	1	25	79	25	0.285
3	1.5	30	118.5	30	0.385
4	2.5	35	158	35	0.522

levels of rough polishing, semi-polishing, and fine polishing are illustrated in Tables 2, 3, and 4, respectively. After polishing experiment, the ultrasonic cleaner is used to clean the inserts at 10 min which are put into the acetone solvent, then are into the absolute ethyl alcohol, and are blew dry with the leaf blower in order to detect surface quality and surface roughness. The surface roughness is regarded as an important index for measuring the polishing quality, the polishing process parameters are optimized by Taguchi's method. Depending on the objectives, Taguchi's method defined three different forms of mean square deviations (i.e., signal-to-noise ratios) including the nominal-the-better, the larger-the-better, and the smaller-the-better. The signal-to-noise ratios can be considered as an average performance characteristic value for each experiment. Three different signal-to-noise ratios corresponding to n experiments are presented as follows.

The nominal-the-better case is

$$Signal\text{-}to\text{-}noise\ ratio = -10 \times \log\left[\frac{1}{n} \times \sum_{i=1}^{n} (x_i - t)^2\right], \quad (1)$$

the larger-the-better case is

$$Signal\text{-}to\text{-}noise\ ratio = -10 \times \log\left(\frac{1}{n} \times \sum_{i=1}^{n} \frac{1}{x_i^2}\right), \quad (2)$$

the smaller-the-better case is

$$Signal\text{-}to\text{-}noise\ ratio = -10 \times \log\left(\frac{1}{n} \times \sum_{i=1}^{n} x_i^2\right), \quad (3)$$

where t is the target value for nominal-the-better cases, x_i is the collected data through experiments, and n represents the number of experiments. Since the objective is to find the optimal parameter combination that minimizes surface roughness, the smaller-the-better equation is chosen for the roughness of surface profiles.

Table 5 Cutting force test conditions

Workpiece material	1Cr18Ni9Ti austenitic stainless steel
Cutting parameters	$v_c = 80$ m/min, $f = 0.15$ mm/r, $a_p = 0.3$, 0.5, 0.8, and 1 mm
	$v_c = 80$ m/min, $a_p = 0.5$ mm, $f = 0.05$, 0.1, 0.15, and 0.2 mm/r
	$f = 0.15$ mm/r, $a_p = 0.5$ mm, $v_c = 40$, 80, 120, and 160 m/min

2.2 Cutting performance test

The cutting performance of the grinding and polished inserts is analyzed by the cutting force test and tool life test. All cutting tests are carried out using CK7525 lathe without coolant, and the inserts are clamped to the commercial tool holder. Combination of the insert and the tool holder resulted in the rake angle of -6.5^o, clearance angle of 6.5^o, tool cutting edge inclination angle -5.5^o, and tool cutting edge angle of 95^o. Firstly, the influence of cutting parameters on the cutting force of the grinding and polished inserts is investigated by single factor test. The cutting force test conditions are shown in Table 5. The Kistler dynamometer of type 9272 and amplifier of type 5019 are used for measuring the cutting force.

Tool life can be defined in terms of the progressive wear which occurs on the tool rake face and/or flank face, i.e., crater wear and flank wear. Flank wear is used to characterize the tool life, which has the major negative influence on the dimensional accuracy and surface finish of the component as well as the stability of the machining process when the flank wear land width VB_B value reach a certain level [13]. Flank wear VB_B value of 0.3 mm is used as the tool life criterion for the continuous turning operations according to ISO standard 3685. But the 1Cr18Ni9Ti austenitic stainless steel is one of the typical difficult-to-machine materials with high impact toughness, elongation, and low thermal conductivity. Through the early trial cutting tests, it is found that in most cases, when the insert flank wear VB_B value has not reached 0.3 mm (usually 0.2–0.3 mm), the other types of wear is very serious, such as groove wear, burnout of tool nose and chipping of cutting edge, which caused the insert to fail. So many enterprises considered the flank wear VB_B value of 0.2 mm as the tool life criterion for the continuous turning

Table 6 Tool life test conditions

Workpiece material	1Cr18Ni9Ti austenitic stainless steel
Cutting parameters	$v_c = 50$ m/min, $f = 0.15$ mm/r, $a_p = 0.5$ mm
	$v_c = 80$ m/min, $f = 0.15$ mm/r, $a_p = 0.5$ mm
	$v_c = 120$ m/min, $f = 0.15$ mm/r, $a_p = 0.5$ mm

Table 7 Experimental data of the rough polishing

No.	A, S_iC abrasive particle (um)	B, Polishing speed (rpm)	C, Polishing pressure (kPa)	D, Polishing time (min)	Surface roughness after polishing Ra (μm)	The SNR value of surface roughness after polishing
1	A1 (26)	B1 (40)	C1 (158)	D1 (35)	0.745	2.557
2	A1 (26)	B2 (50)	C2 (177.8)	D2 (50)	0.304	10.343
3	A1 (26)	B3 (60)	C3 (197.5)	D3 (65)	0.781	2.147
4	A2 (22)	B1 (40)	C2 (177.8)	D3 (65)	0.445	7.033
5	A2 (22)	B2 (50)	C3 (197.5)	D1 (50)	0.768	2.293
6	A2 (22)	B3 (60)	C1 (158)	D2 (35)	0.652	3.715
7	A3 (18)	B1 (40)	C3 (197.5)	D2 (50)	0.529	5.531
8	A3 (18)	B2 (50)	C1 (158)	D3 (65)	0.576	4.792
9	A3 (18)	B3 (60)	C2 (177.8)	D1 (35)	0.641	3.863

Table 8 Experimental data of semi-polishing

No.	A, SiC abrasive particle (um)	B, Polishing speed (rpm)	C, Polishing pressure (kPa)	D, Polishing time (min)	Surface roughness after polishing Ra (μm)	The SNR value of surface roughness after polishing
1	A1 (10)	B1 (30)	C1 (98.75)	D1 (25)	0.506	5.917
2	A2 (10)	B2 (35)	C2 (118.5)	D2 (35)	0.374	8.543
3	A3 (10)	B3 (40)	C3 (138.25)	D3 (45)	0.243	12.288
4	A2 (7)	B1 (30)	C2 (118.5)	D3 (45)	0.287	10.842
5	A2 (7)	B2 (35)	C3 (138.25)	D1 (35)	0.439	7.151
6	A2 (7)	B3 (40)	C1 (98.75)	D2 (25)	0.456	6.821
7	A3 (5)	B1 (30)	C3 (138.25)	D2 (35)	0.346	9.218
8	A3 (5)	B2 (35)	C1 (98.75)	D3 (45)	0.307	10.257
9	A3 (5)	B3 (40)	C2 (118.5)	D1 (25)	0.425	7.432

Table 9 Experimental data of fine polishing

No.	A, Diamond powder (um)	B, Polishing speed (rpm)	C, Polishing pressure (kPa)	D, Polishing time (min)	E, Abrasive concentration (ct/ml)	Surface roughness after polishing Ra (μm)	The SNR value of surface roughness after polishing
1	A1 (0.5)	B1 (20)	C1 (39.5)	D1 (20)	E1 (0.181)	0.058	24.731
2	A1 (0.5)	B2 (25)	C2 (79)	D2 (25)	E2 (0.285)	0.049	26.196
3	A1 (0.5)	B3 (30)	C3 (118.5)	D3 (30)	E3 (0.385)	0.016	35.918
4	A1 (0.5)	B4 (35)	C4 (158)	D4 (35)	E4 (0.522)	0.045	26.936
5	A2 (1)	B1 (20)	C2 (79)	D3 (30)	E4 (0.522)	0.024	32.396
6	A2 (1)	B2 (25)	C1 (39.5)	D4 (35)	E3 (0.385)	0.067	23.479
7	A2 (1)	B3 (30)	C4 (158)	D1 (20)	E2 (0.285)	0.073	22.734
8	A2 (1)	B4 (35)	C3 (118.5)	D2 (25)	E1 (0.181)	0.032	29.897
9	A3 (1.5)	B1 (20)	C3 (118.5)	D4 (35)	E2 (0.285)	0.047	26.558
10	A3 (1.5)	B2 (25)	C4 (158)	D3 (30)	E1 (0.181)	0.037	28.636
11	A3 (1.5)	B3 (30)	C1 (39.5)	D2 (25)	E4 (0.522)	0.049	26.196
12	A3 (1.5)	B4 (35)	C2 (79)	D1 (20)	E3 (0.385)	0.039	28.179
13	A4 (2.5)	B1 (20)	C4 (158)	D2 (25)	E3 (0.385)	0.037	28.636
14	A4 (2.5)	B2 (25)	C3 (118.5)	D1 (20)	E4 (0.522)	0.032	29.897
15	A4 (2.5)	B3 (30)	C2 (79)	D4 (35)	E1 (0.181)	0.049	26.196
16	A4 (2.5)	B4 (35)	C1 (39.5)	D3 (30)	E2 (0.285)	0.079	22.047

Table 10 SNR level response of rough polishing surface roughness

SNR of rough polishing surface roughness (dB)				
Levels	A, S_iC abrasive particle	B, Polishing speed	C, Polishing pressure	D, Polishing time
1	5.016	5.040	3.688	2.904
2	4.347	5.809	7.080	6.530
3	4.729	3.242	3.324	4.657

Table 11 SNR level response of semi-polishing surface roughness

SNR of semi-polishing surface roughness (dB)				
Levels	A, S_iC abrasive particle	B, Polishing speed	C, Polishing pressure	D, Polishing time
1	8.916	8.659	7.665	6.833
2	8.271	8.650	8.939	8.194
3	8.969	8.847	9.552	11.129

1Cr18Ni9Ti austenitic stainless steel. The tool life test conditions are shown in Table 6.

Tool life can be characterized by the working time of the insert without adjustment or replacement, the number of machined parts, the length of the tool path, or the area of the machined surface [14]. In the paper, the tool life has been defined as the elapsed machining time when the flank wear reaches the allowed limit equal to the criterion 0.2 mm. The ultra-depth of field microscope (HIROX) is used to observe the insert rake face and flank wear at every 2 min.

3 Results and discussions

3.1 Cemented carbide inserts processed with the CMP method

According to the orthogonal experiment scheme, the $L9$ (3^4) orthogonal table is selected to rough polishing and semi-polishing experiment. The $L16$ (4^5) orthogonal table is selected to fine polishing experiment. The smaller-the-better (Eq. (3)) is selected for the surface roughness. Taguchi's method, which applied a signal-to-noise ratio to represent the quality characteristic, obtained an optimal process parameter combination through finding the largest signal-to-noise ratio. The experimental data are listed in Tables 7, 8, and 9.

According to Tables 7, 8, and 9, the responses of signal-to-noise ratios for different levels of factors are listed in Tables 10, 11, and 12. A1B2C2D2 is the optimal parameter combination for rough polishing process which gives the largest sum of signal-to-noise ratio. Namely, the optimal parameter combination is with SiC abrasive particle size of 26 um, polishing speed of 50 rpm, polishing pressure of 177.8 kPa, and polishing time of 50 min. In the same way, A3B3C3D3 is the optimal parameter combination for the semi-polishing processes. Namely, the optimal parameter combination is with S_iC abrasive particle size of 5 um, polishing speed of 40 rpm, polishing pressure of 138.25 kPa, and polishing time of 45 min. A1B1C3D3E3 is the optimal parameter combination for the fine polishing process. Namely, the optimal parameter combination is with diamond powder size of 0.5 um, polishing speed of 20 rpm, polishing pressure of 118.5 kPa, and polishing time of 30 min, abrasive concentration of 0.385 ct/ml.

Finally, the optimal combination for rough polishing, semi-polishing, and fine polishing are used to prepare better surface quality of the inserts. The ultra-depth of field microscope (HIROX) is used to observe the surface topography of the grinding and polished inserts under the condition of 500 times, which are shown in Figs. 3 and 4. It is found that there are a lot of deep scratches on the rake face of the grinding insert. There is few scratch on the rake face of the polished insert. So, the quality of rake face of the polished insert is better than the grinding insert.

The atomic force microscope (AFM) is used to observe the rake face topography and roughness of the polished insert, which are shown in Figs. 5 and 6. It is found that the rake face of the polished insert is extremely flat, and 14.399 nm Ra on the rake face is obtained.

3.2 Cutting force

Cutting force is one of the important physical phenomena in the cutting process and is also one of the important contents of cutting performance of the grinding and polished inserts.

Table 12 SNR level response of fine polishing surface roughness

Levels	A, Diamond powder	B, Polishing speed	C, Polishing pressure	D, Polishing time	E, Abrasive concentration
1	28.445	28.080	24.113	26.385	27.365
2	27.127	27.052	28.242	27.731	24.384
3	27.392	27.761	30.568	29.749	29.053
4	26.694	26.765	26.736	25.792	28.856

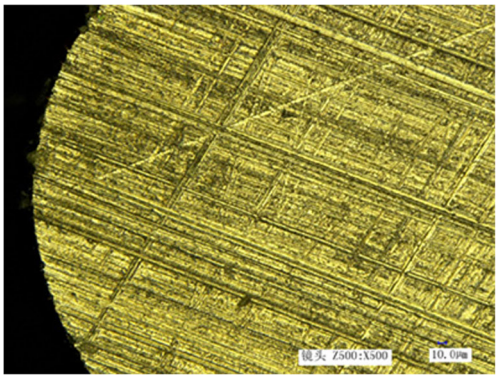

Fig. 3 Grinding insert rake face

There are many factors that affect the cutting force in the cutting process, such as cutting parameters, tool geometry parameters, tool surface quality, and so on, especially the tool surface quality has an important influence on the cutting force. The friction coefficient between the tool surface and the workpiece material affects the change of the friction force, and directly affects the change of cutting force, further affects the tool wear and breakage and the machined surface quality. Hence, the analysis of cutting force signal is getting more and more important. The single factor test is carried out to study the influence of the surface quality of the grinding and polished inserts on the cutting force. The main cutting force F_z, back force F_y, and feed force F_x are measured by the dynamometer. The variations of cutting force with different cutting parameters are shown in Figs. 7, 8, and 9, respectively.

It is found that with the increase of depth of cut a_p and feed rate f, the main cutting force F_z of the grinding and polished inserts increased, and the main cutting force F_z decreased with the increase of the cutting speed v_c, but when the cutting speed is more than 120 m/min, the cutting force F_z decreased slowly. In general, the cutting force of the polished insert is smaller than the grinding insert with the same cutting condition. The reason is that the roughness of the polished insert rake face is lower than the grinding insert, and the cutting edge of the polished insert is sharp. Therefore, the friction force between

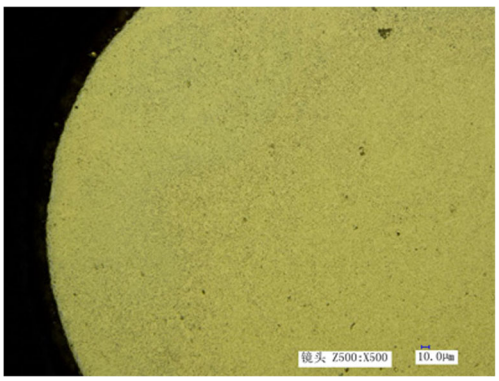

Fig. 4 Polished insert rake face

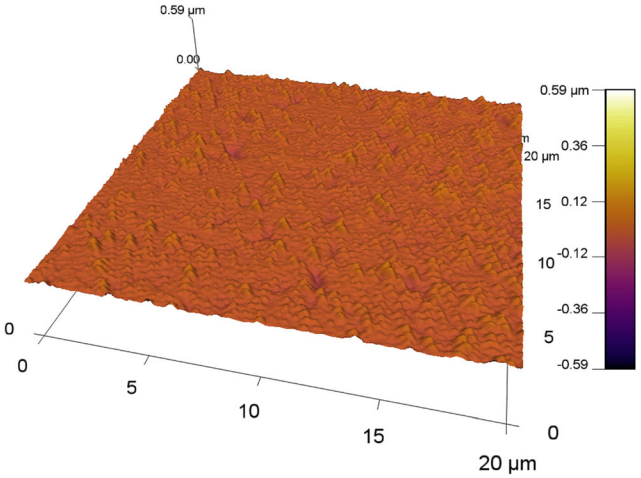

Fig. 5 Rake face topography of the polished insert

the rake face and the chip is small, and the cutting force is also small.

The relationship between the cutting parameters and the cutting force can be expressed by the following formula:

$$F = C_F a_p^{b_1} f^{b_2} v^{b_3} \tag{4}$$

where F is the cutting force (N), C_F is the correlation coefficient, b_1 is the effect index of cutting depth a_p on the cutting force, b_2 is the effect index of feed rate f on the

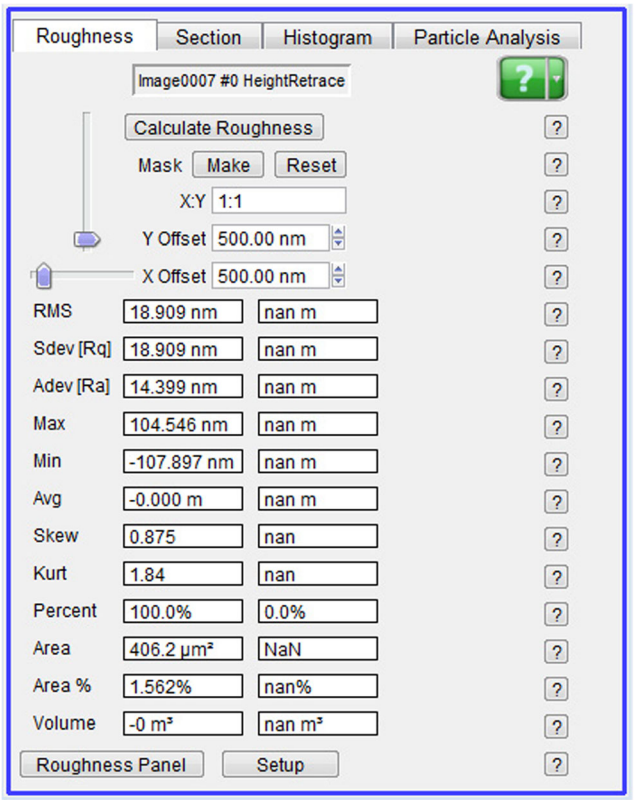

Fig. 6 Rake face roughness of the polished insert

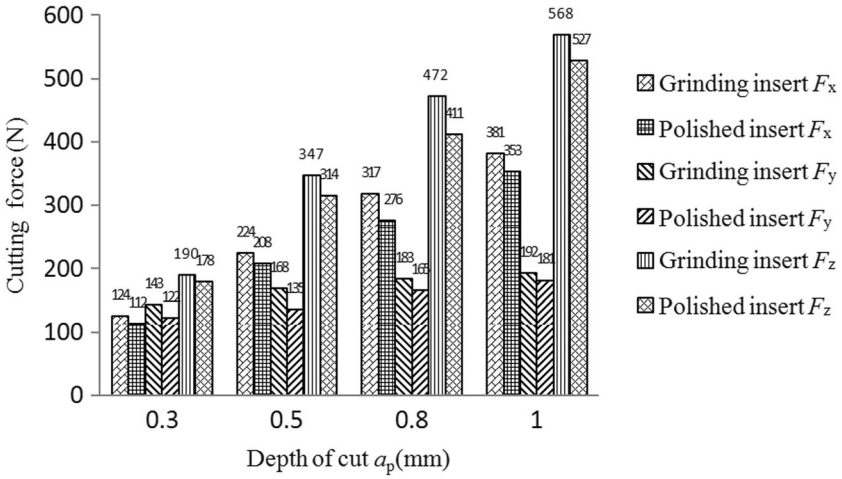

Fig. 7 Effect of depth of cut a_p on the cutting force of the grinding and polished inserts

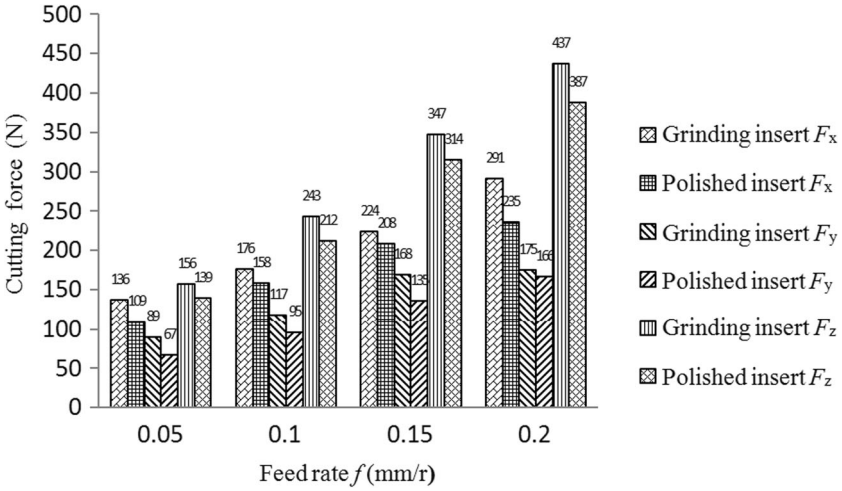

Fig. 8 Effect of feed rate f on the cutting force of the grinding and polished inserts

cutting force, and b_3 is the effect index of cutting speed v_c on the cutting force.

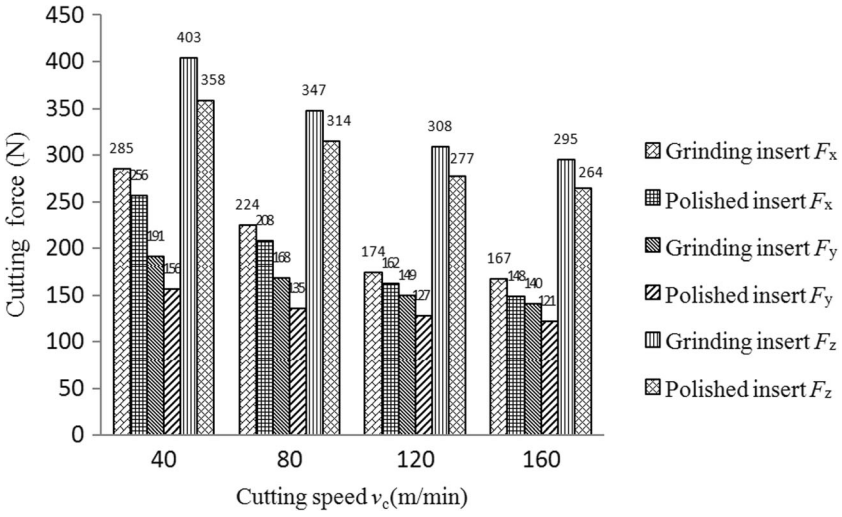

Fig. 9 Effect of cutting speed v_c on the cutting force of the grinding and polished inserts

According to the cutting force data, the empirical formula of cutting force can be obtained by regression analysis, which is shown as follows.

The grinding insert:

$$\begin{cases} F_x = 5955 a_p^{0.885} f^{0.473} v^{-0.41} & R^2 = 0.9622 \\ F_y = 1450 a_p^{0.25} f^{0.556} v^{-0.221} & R^2 = 0.962 \\ F_z = 6209 a_p^{0.85} f^{0.718} v^{-0.222} & R^2 = 0.977 \end{cases} \quad (5)$$

The polished insert:

$$\begin{cases} F_x = 5910 a_p^{0.89} f^{0.537} v^{-0.405} & R^2 = 0.9786 \\ F_y = 1432 a_p^{0.352} f^{0.682} v^{-0.184} & R^2 = 0.9809 \\ F_z = 5559 a_p^{0.835} f^{0.731} v^{-0.217} & R^2 = 0.9812 \end{cases} \quad (6)$$

The calculated cutting force agreed well with the experiment results, and the determination coefficient R^2 value of the above regression results is good. As for the feed force F_x and cutting force F_z of the grinding and polished inserts, it can be seen that depth of cut a_p played a predominant role, followed by feed rate f and cutting speed v_c. But as for the back force F_y, it can be seen that feed rate f played a predominant role, followed by depth of cut a_p and cutting speed v_c.

3.3 Tool life

During the cutting test, the depth of cut a_p and feed rate f are kept constant at 0.5 mm and 0.15 mm/r, respectively, and the cutting speed v_c varied at 50, 80, and 120 m/min. The flank wear VB_B values of the grinding and polished inserts are measured and the average values are plotted as a function of cutting time with different cutting speeds, which are shown in Figs. 10 and 11, respectively.

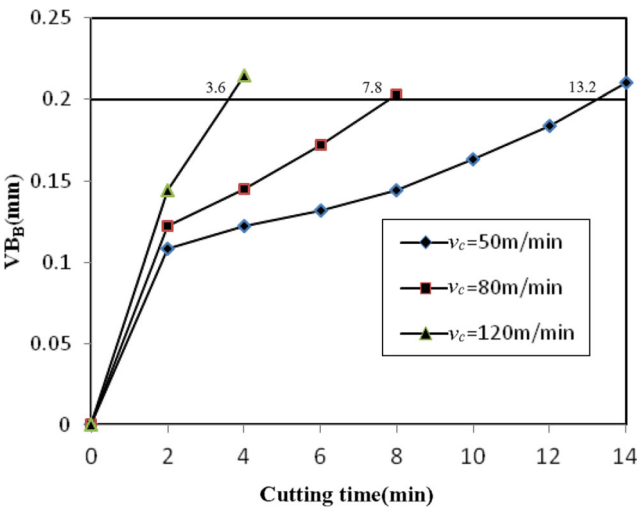

Fig. 10 Flank wear VB_B values of the grinding insert as a function of cutting time under different cutting speeds

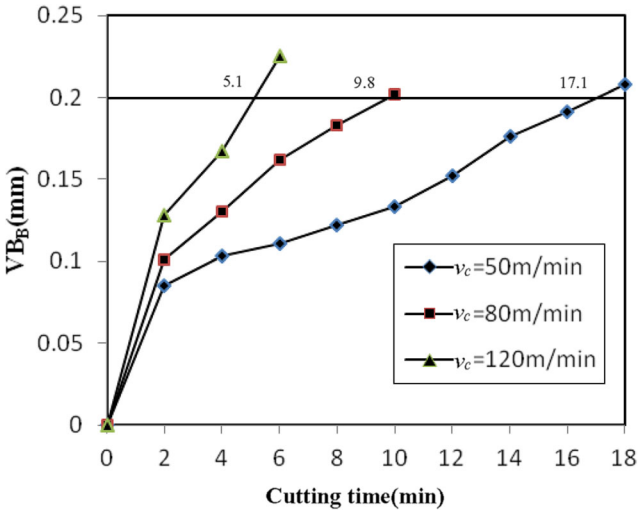

Fig. 11 Flank wear VB_B values of the polished insert as a function of cutting time under different cutting speeds

It is found that the larger the cutting speed means more serious thermal, mechanical, and chemical impact on the cutting tool. Therefore, it can be concluded that the flank wear VB_B values of the grinding and polished inserts increased with the increase of cutting speed v_c, namely the cutting time of the grinding and polished inserts decreased with the increase of cutting speed v_c. Under the same cutting speed, the cutting time of the polished insert is longer than that of the grinding insert, and the average life of the polished insert is 32.3% longer than that of the grinding insert.

3.4 Tool wear

During the cutting test, the depth of cut a_p and feed rate f are kept constant at 0.5 mm and 0.15 mm/r, respectively, and the cutting speed v_c varied at 50, 80, and 120 m/min. The ultra-depth of field microscope is used to observe the insert rake and flank wear. The rake and flank wear morphology of the polished and grinding inserts is shown in Fig. 12, which are magnified 160 times in the ultra-depth of field microscope.

Figure 12a, b shows that there is adhesive wear on the grinding insert rake face during cutting 1Cr18Ni9Ti austenitic stainless steel with the cutting speed of 50 m/min, and notch wear can be seen on the flank face due to the friction between the hard particles of workpiece and grinding insert flank face. From Fig. 12c, d, it is found that with the increase of cutting speed increased to 80 m/min, the adhesive wear became obvious on the rake face due to the high speed flow of chips, especially adjacent to the tool edge, and notch wear is also the main wear form of the flank face. From Fig. 12e, it is found that with the increase of cutting speed increased to 120 m/min, the adhesive

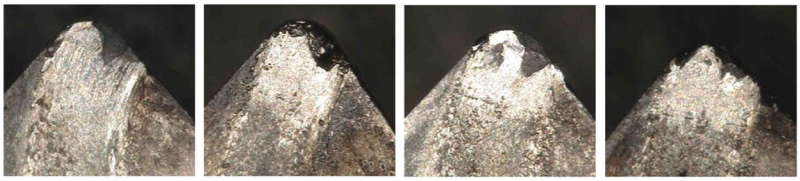

(a) Rake wear morphology of the grinding insert with cutting speed v_c=50m/min.

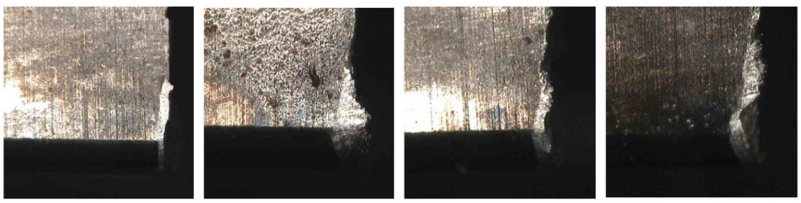

(b) Flank wear morphology of the grinding insert with cutting speed v_c =50m/min.

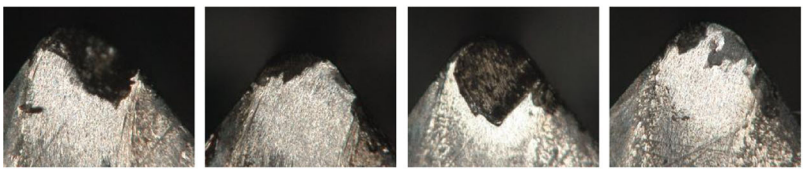

(c) Rake wear morphology of the grinding insert with cutting speed v_c =80m/min.

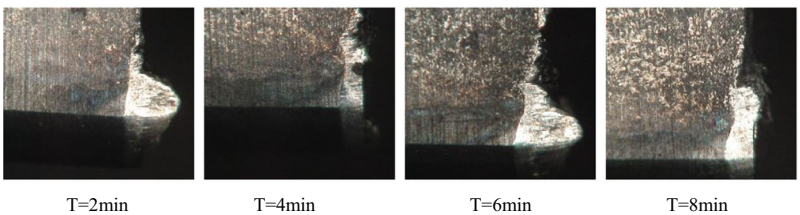

(d) Flank wear morphology of the grinding insert with cutting speed v_c =80m/min.

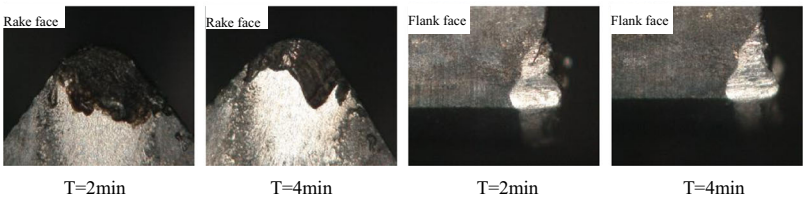

(e) Rake and wear morphology of the grinding insert with cutting speed v_c =120m/min.

Fig. 12 Rake and flank wear morphology of the grinding and polished inserts with different cutting speeds. (**a**) Rake wear morphology of the grinding insert with cutting speed $v_c = 50$ m/min. (**b**) Flank wear morphology of the grinding insert with cutting speed $v_c = 50$ m/min. (**c**) Rake wear morphology of the grinding insert with cutting speed $v_c =$ 80 m/min. (**d**) Flank wear morphology of the grinding insert with cutting speed $v_c = 80$ m/min. (**e**) Rake and wear morphology of the grinding insert with cutting speed $v_c = 120$ m/min. (**f**) Rake wear morphology of the polished insert with cutting speed $v_c = 50$ m/min. (**g**) Flank wear morphology of the polished insert with cutting speed $v_c =$ 50 m/min. (**h**) Rake wear morphology of the polished insert with cutting speed $v_c = 80$ m/min. (**i**) Flank wear morphology of the polished insert with cutting speed $v_c = 80$ m/min. (**j**) Rake and wear morphology of the polished insert with cutting speed $v_c = 120$ m/min

wear appeared more serious on the rake face due to the high speed flow of chips, and notch wear can be seen on the flank face.

Figure 12f, g shows that there is similarly adhesive wear on the polished insert rake face during cutting 1Cr18Ni9Ti austenitic stainless steel with the cutting speed of 50 m/min, but

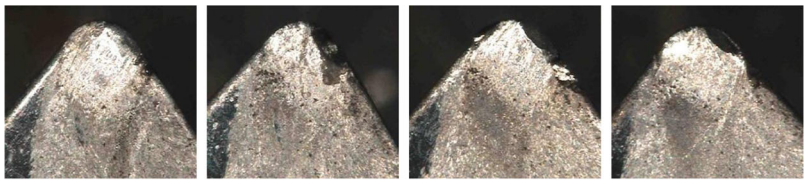

(f) Rake wear morphology of the polished insert with cutting speed v_c =50m/min.

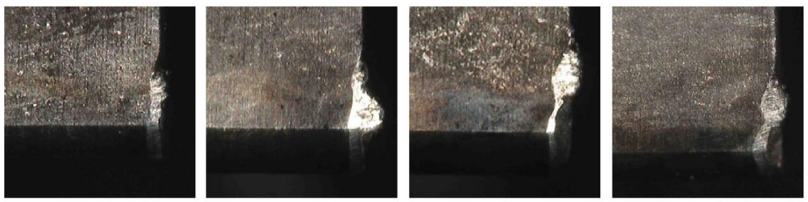

(g) Flank wear morphology of the polished insert with cutting speed v_c =50m/min.

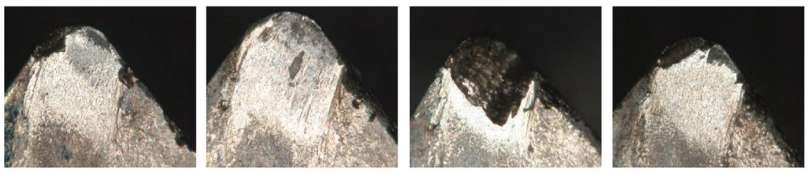

(h) Rake wear morphology of the polished insert with cutting speed v_c =80m/min.

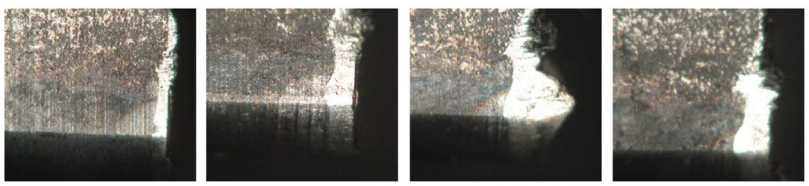

(i) Flank wear morphology of the polished insert with cutting speed v_c =80m/min.

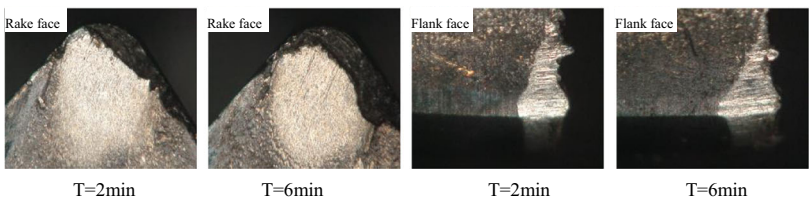

(j) Rake and wear morphology of the polished insert with cutting speed v_c =120m/min.

Fig. 12 (continued)

the adhesive wear on the rake face less serious than the grinding insert. In addition, at the end of the machining, tool materials spalling after the adhesive of workpiece materials can be seen on the rake face, which results in the micro chipping on the cutting edge. Figure 12h, i shows that with the increase of cutting speed increased to 80 m/min, the adhesive wear became obvious, but the height of the adhesive layer is lower than that of the grinding insert, and notch wear and chipping of cutting edge can be seen on the flank face. Figure 12j shows that with the increase of cutting speed increased to 120 m/min, the adhesive wear appeared more serious, and the height of the adhesive layer is also lower than that of the grinding insert, and the notch wear is the main wear form of the polished insert flank face.

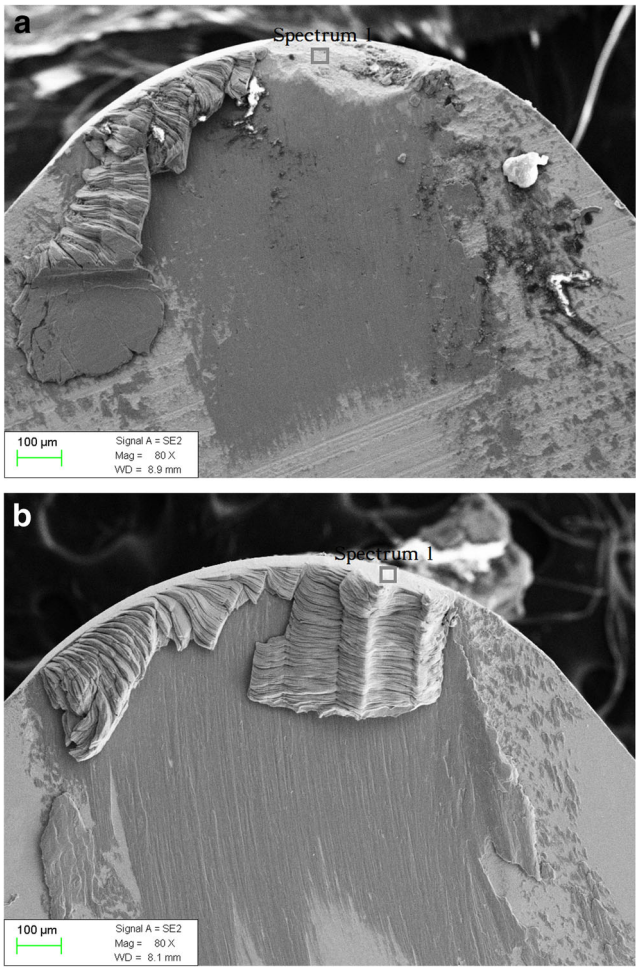

Fig. 13 Rake wear morphology of the grinding and polished inserts with cutting speed v_c as 80 m/min, (**a**) grinding insert and (**b**) polished insert

The scanning electron microscopy (SEM) and the energy dispersive spectrometer (EDS) are used to observe the rake wear of the polished and grinding inserts with a_p as 0.5 mm, f as 0.15 mm/r, and v_c as 80 m/min, which are shown in Figs. 13 and 14, respectively.

Figure 14 shows the EDS spectrum of the worn rake faces of the grinding and polished inserts with a_p as 0.5 mm, f as 0.15 mm/r, and v_c as 80 m/min. Fe, Cr, Ni, O, C, Co, and W content can be seen on the worn rake faces of the grinding and polished inserts. The existence of Fe, Ni, and Cr elements indicated the adhesion of 1Cr18Ni9Ti workpiece materials on the tool insert due to the pressure and heat produced during cutting process. The existence of O element indicated the area near the insert corner occurred oxidation wear. There are Fe, Cr, Ni, Co, and W peaks on the worn rake face of the grinding and polished inserts, revealing the combination of adhesive wear and abrasive wear. Considering the wear morphology and EDS peaks intensity, the adhesive wear, abrasive wear, and minor oxidation wear appear on the rake face of the polished insert, and the combination of more serious adhesive wear, abrasive wear, and oxidation wear exist on the rake face of the grinding insert.

4 Conclusions

This work has investigated the chemical mechanical polishing process of insert surfaces to improve the insert quality. The

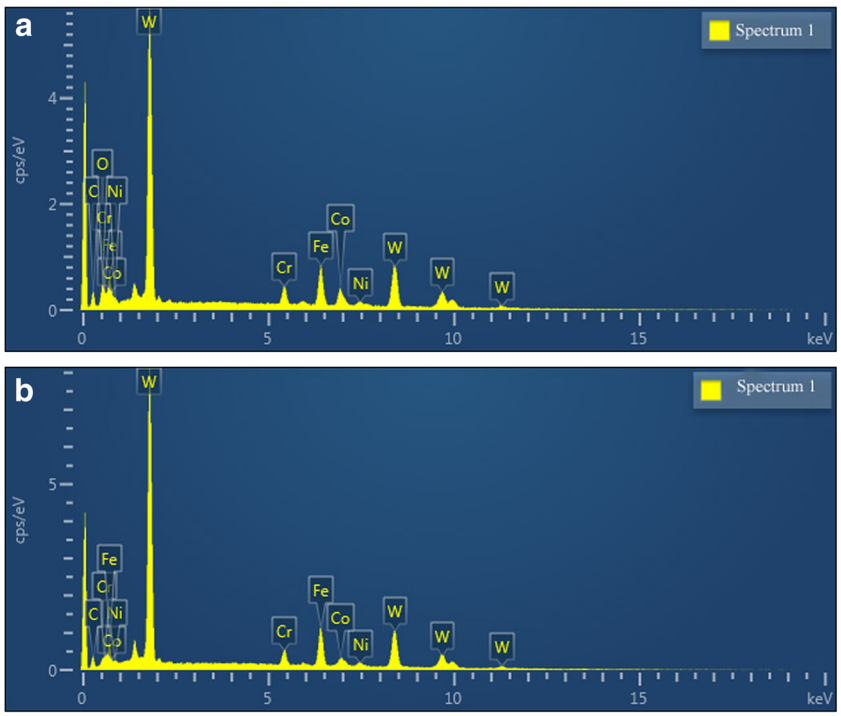

Fig. 14 EDS spectrum of the worn rake face of the grinding and polished inserts, (**a**) grinding insert and (**b**) polished insert

parameters of the chemical mechanical polishing process are optimized with orthogonal experiments and Taguchi's method. The surface finish Ra of the insert rake face is 14.399 nm. The inserts made with the conventional grinding and the CMP methods are used to lathe 1Cr18Ni9Ti austenitic stainless steel. Under the same cutting conditions, the cutting forces of the polished insert is less than those of the grinding insert, the cutting time of the polished insert is longer than that of the grinding insert, and the average life of the polished insert is 32.3% longer than that of the grinding insert. The polished insert rake face has less adhesive, abrasive, and minor oxidation wear, compared to the wear of the grinding insert rake face. This study is useful to advance research on improving the insert quality.

Acknowledgments The work is carried out using the unique facilities of the Zhuzhou Cemented Carbide Cutting Tools Co. Ltd. of China, which the authors greatly appreciate.

Funding information This work is supported by the key programs of Hunan Provincial Department of science and technology of China (No. 2016GK2014), Hunan Provincial Natural Science Foundation of China (No. 2017JJ4055), and Hunan Provincial Innovation Foundation for Postgraduate of China (No. CX2016B231), which the authors greatly appreciate.

References

1. Sugihara T, Enomoto T (2015) High speed machining of Inconel 718 focusing on tool surface topography of CBN tool. Procedia Manuf 1:675–682. https://doi.org/10.1016/j.promfg.2015.09.010
2. Luo SY, Liu YC, Chou CC, Chen JP (2001) Performance of power filled resin-bonded diamond wheels in the vertical dry grinding of tungsten carbide. J Mater Process Technol 118(1–3):329–336. https://doi.org/10.1016/S0924-0136(01)00861-5
3. Hegeman JBJW, Hosson JTMD, With G (2001) Grinding of WC–Co hardmetals. Wear 248(1–2):187–196. https://doi.org/10.1016/S0043-1648(00)00561-5
4. Koshy P, Jain VK, Lal GK (1997) Grinding of cemented carbide with electrical spark assistance. J Mater Process Technol 72(1):61–68. https://doi.org/10.1016/S0924-0136(97)00130-1
5. Kim JD, Lee ES (1999) A study of the mirror-like grinding of sintered carbide with optimum in-process electrolytic dressing. Int J Adv Manuf Technol 15(9):615–623. https://doi.org/10.1007/s001700050110
6. Yin L, Spowage AC, Ramesh K, Huang H, Pickering JP, Vancoille EYJ (2004) Influence of microstructure on ultraprecision grinding of cemented carbides. Int J Mach Tool Manu 44(5):533–543. https://doi.org/10.1016/j.ijmachtools.2003.10.022
7. Ali I, Roy SR, Shinn G (1994) Chemical-mechanical polishing of interlayer dielectric: a review. Solid State Technol 37(10):63–70
8. Malik F, Hasan M (1995) Manufacturability of the CMP process. Thin Solid Films 270(1–2):612–615. https://doi.org/10.1016/0040-6090(96)80083-6
9. Shi X, Rock SE, Turk MC, Roy D (2012) Minimizing the effects of galvanic corrosion during chemical mechanical planarization of aluminum in moderately acidic slurry solutions. Mater Chem Phys 136(2–3):1027–1037. https://doi.org/10.1016/j.matchemphys.2012.08.044
10. Luan X, Liu Y, Wang C, Niu X, Wang J, Zhang W (2016) A study on exploring the alkaline copper CMP slurry without inhibitors to achieve high planarization efficiency. Microelectron Eng 160:5–11. https://doi.org/10.1016/j.mee.2016.02.044
11. Seo J, Kim JH, Lee M, You K, Moon J, Lee DH, Pailk U (2017) Multi-objective optimization of tungsten CMP slurry for advanced semiconductor manufacturing using a response surface methodology. Mater Des 117:131–138. https://doi.org/10.1016/j.matdes.2016.12.066
12. Ozdemir Z, Ozdemir A, Basim GB (2016) Application of chemical and mechanical polishing process on titanium based implants. Mater Sci Eng 68:383–396. https://doi.org/10.1016/j.msec.2016.06.002
13. Arsecularatne JA, Zhang LC, Montross C (2006) Wear and tool life of tungsten carbide, PCBN and PCD cutting tools. Int J Mach Tool Manu 46(5):482–491. https://doi.org/10.1016/j.ijmachtools.2005.07.015
14. Astakhov VP (2004) The assessment of cutting tool wear. Int J Mach Tool Manu 44(6):637–647. https://doi.org/10.1016/j.ijmachtools.2003.11.006